A robust and frugal model of biomass pyrolysis in the range 100–800 °C: Inverse analysis of DAEM parameters, validation on static tests and determination of heats of reaction

Patrick Perré, Yong Tian, Pin Lu, Barbara Malinowska, Jamila El Bekri, Julien Colin

Version of Record: https://www.sciencedirect.com/science/article/pii/S0016236120326880
Manuscript_1570983060b5fda6785723452cff2129

A robust and frugal model of biomass pyrolysis in the range 100-800°C: inverse analysis of DAEM parameters, validation on static tests and determination of heats of reaction

Patrick Perré[a,b,*], Yong Tian[b], Pin Lu[a], Barbara Malinowska[b], Jamila El Bekri[b], Julien Colin[a,b]

[a] *LGPM, CentraleSupélec, Centre Européen de Biotechnologie et de Bioéconomie (CEBB), 3, rue des Rouges Terres, 51110 Pomacle, France*
[b] *LGPM, CentraleSupélec, Université Paris-Saclay, Plateau du Moulon, 91190 Gif-sur-Yvette, France*

Abstract

This paper presents a robust and frugal Distributed Activation Energy Model to simulate pyrolysis of lignocellulosic biomass (spruce and poplar) over a wide range of temperature and residence time. The learning database consists of dynamic TGA-DSC experiments performed up to 800°C at four heating rates (1, 2, 5 and 10 K/min). By employing one non-symmetrical distribution, three distributions and only 9 independent parameters were needed to correctly fit the experimental data : a Gaussian distribution for hemicelluloses, a Gaussian function degenerated into a Dirac function for cellulose and a gamma function degenerated into an exponential function for lignins.

The robustness of the model was successfully validated with 2-hours isothermal tests (250°C to 500°C with increments of 50°C). The heats of reaction were determined using the heat flux measured under fast dynamic conditions, thus reducing the crucial problem of baseline drift. The prediction potential of the model is highlighted by two examples: pathway in the Van Krevelen's diagram and control of the temperature rise to limit the heat source due to reactions.

The model equations, the discretization and computational implementation, as well as the complete set of model parameters are presented in great detail, so that the reader can use them for process modelling, including the crucial concern of thermal runaway occurring in large particles or packed beds.

Keywords: computational modeling, identification, poplar, prediction, spruce, validation

*Corresponding author
Email address: patrick.perre@centralesupelec.fr (Patrick Perré)

1. Introduction

Biofuel derived from biomass is a source of renewable energy for transportation (Demirbas, 2008). Technologies based on thermal processes are part of the conversion route from biomass to biofuel and energy source, among which pyrolysis is often the first step before combustion, gasification or grinding. During this process, biomass decomposes under inert atmosphere in the form of gas, bio-oil and char.

Thermogravimetric analysis (TGA) is the most common analytical method for experimental investigation of biomass decomposition (Grønli et al., 1999; Antal et al., 1998; White et al., 2011). TGA detects online the evolution of mass loss, a good indicator of the alterations of biomass properties (Almeida et al., 2010). The earliest kinetics works were performed at isothermal conditions and the decomposition rates were formulated over a certain range of temperature and pre-heating conditions (Thurner and Mann, 1981; Ward and Braslaw, 1985; Wagenaar et al., 1993). Dynamic tests are, however, more widely-used for their ability to investigate a wide range of temperature and to use analytical solutions for kinetics determination. On the contrary, when analysed using analytical solutions, isothermal kinetics suffered from the noticeable weight loss during warm-up time (Brachi et al., 2015; Lv et al., 2012; Cai et al., 2013b).

The earliest kinetics works have formulated the degradation kinetics of lignocellulosic biomass or their components (cellulose, hemicelluloses and lignins) as a set of competitive and/or consecutive reactions (Ramiah, 1970; Alves and Figueiredo, 1989; Varhegyi et al., 1989, 1994; Di Blasi and Lanzetta, 1997; Fisher et al., 2002; Rousset et al., 2006).

Currently, Distributed Activation Energy Model (DAEM) became the standard modelling tools for thermal degradation of biomass. This concept was developed by Vand (1943) to model pyrolysis of coal and was later applied to lignocellulosic biomass (Teng and Wei, 1998; Shen et al., 2011; Cai et al., 2013a). This model represents the decomposition process as a continuous series of independent and parallel reactions with different activation energies which were further described by continuous distribution functions. Analytical method were first derived to extract the distribution functions from experimental data (Miura, 1995). In the case of biomass, the actual decomposition process involved

complicated steps with different activation energy distributions. As multi-distribution models are required, the common practice is to use a computational solution to solve a full set of distributions of any shape.

This kind of model is among the most comprehensive models for describing pyrolysis kinetics of lignocellulosic biomass and its components (Cai et al., 2014; Xu et al., 2018) and already proved its prediction potential for tests that were not include in the learning database (Cavagnol et al., 2015). Recent DAEM developments include a whole set of works using multiple normal distributed activation energy model. Depending on the experimental database, and probably also on the authors' expectations, two (de Caprariis et al., 2015), three (Chen et al., 2015, 2016) or even five (Lin et al., 2018) normal distributions are proposed to get a good fit with the experimental data.

Many works were devoted to the refinement of the pre-exponential factor A (also called the frequency factor). Some authors proposed this factor to depend on temperature : $A = A_0 T^n$ (Cai and Liu, 2008). Sfakiotakis and Vamvuka (2015) proposed this factor to depend on the heating rate (HR). A linear relationship between the logarithm of the pre-exponential factor A and the mean value of the activation energy distribution was also introduced (Czajka et al., 2016; Xu et al., 2018). In all proposals, the authors claimed, and proved, that this allows the quality of the fit to be improved. This is not so surprising as any additional degree of freedom in the inverse procedure necessarily reduces the residues. Other improvements concerned the shape of the distribution functions. As Gaussian distributions are still widely used, other shapes, such as Logistic, Uniform and Weibull function have been proposed (Cai et al., 2014; Li et al., 2019).

However, the complexity of this approach, namely the number of degrees of freedom, together with the well-known compensation effect make it difficult to propose an unambiguous set of model parameters (Chornet and Roy, 1980; Soria-Verdugo et al., 2015). Thus any kinetics model based on inverse analysis should include two steps : i) Parameters identification on a learning database and ii) Model validation using alternating time-temperature pathways.

Yet, to the best of our knowledge, we found only two works that includes the validation step. Lin et al. (2019) used experimental data performed at 20 K/min as learning database

and used the identified parameters to successfully predict tests performed at 15 K/min and 25 K/min. In Li et al. (2019), the same team used the identified model to predict the distribution of activation energies.

Besides, the heats of reaction are of utmost importance to properly simulate the intricate heat and mass coupling occurring during the thermo-chemical process, either inside particles large enough for the fields to be non-uniform (Turner et al., 2010) or in a bed of particles (Perré et al., 2013; Cavagnol et al., 2015). Unfortunatly, the literature remains sparse regarding the heats of reaction, even though this information is of crucial importance to consider the thermal runaway that is likely to appear in industrial processes. Former studies on the determination of reaction enthalpies encountered difficulties like large errors in pyrolysis calculation (Reed and Gaur, 1997), uncertainty and unknown accuracies (And and Brown, 2003). The lack of precision is often attributed to the experimental conditions, which includes the sample size, the nature of the atmosphere, and the presence of impurities. To gain accuracy, differential scanning calorimetry (DSC) could to be an effective way (Rath et al., 2003). Note however that, in this case, it is difficult to rely the heat flux to the mass loss evolution, hence to determine reaction enthalpies. The published reaction enthalpies range from -3800 to 418 kJ/kg for wood (Tinney, 1965; Kung and Kalelkar, 1973; Ramiah, 1970; Rath et al., 2003), from -510 to 322 kJ/kg for cellulose , from -455 to 79 kJ/kg for lignin and from -700 to 42 kJ/kg for hemicelluloses (Beall, 1971). Such large variations, ranging from endothermic to exothermic, point out the real difficulty to determine these heats of reaction (Rath et al., 2003; Di Blasi, 2008). A value of -850 kJ/kg was determined by inverse analysis for the degradation of hemicelluloses in (Turner et al., 2010). This value was tuned to predict the correct thermal runaway in a coupled heat and mass transfer computational code. However, one must keep in mind that this value is strongly tied to the kinetics model implemented in the code. Anyway, the temperature overshot measured inside the macro-particle (Turner et al., 2010) or in a packed-bed (Di Blasi et al., 2013; Cavagnol et al., 2015) proves that pyrolysis involves exothermic reactions, which is in contradiction with other published works (Wang et al., 2017a; Mishra and Mohanty, 2018).

In the present paper, we propose a robust DAEM model to simulate pyrolysis of two

types of lignocellulosic products (spruce and poplar) over a wide range of temperature levels and treatment durations. The inspiration for this work is i) to find best compromise between the sobriety of the number of parameters to be identified and the robustness of the model validated on very distinct experimental data and ii) to use to the DSC signal to identify heats of reaction. The whole procedure is explained in detail to allow the reader to implement the modelling strategy for its own needs. The full dataset is supplied for poplar and spruce (kinetics parameters and reaction enthalpies), which can be used for the simulation of biomass pyrolysis, including thermal runaway likely to occur in large particle or packed beds of particles.

2. Materials and methods

Poplar (*Populus euramerican* cv. I-214) was selected from a 17-year-old tree (cottonwood native black poplar in the Po Valley, female). The spruce tree (*Picea abies*) was about 31-year-old and selected from the Brin forest, Champenoux, France. The choice of these species was motivated by two objectives: i) The selection of potential species for biofuel production due to their availability ii) the scientific interest of comparing hardwoods and softwoods in regard to their pyrolysis behaviour. Healthy trees with no apparent injury were used. Stem disks were cut from each tree at 6 m above the ground. Small blocks were selected from these disks avoiding the sapwood and the pith regions. All samples were milled by using a grinder (IKA M20 Universal mill) and subsequently sieved. The particle size fraction from 0.063 to 0.08 mm was selected in order to neglect internal heat and mass transfer limitations during pyrolysis. The ultimate analysis was conducted in elementary analyzer (FLASH 2000 CHNS/O, Thermo Fisher Scientific) and proximate analysis was based on standard methods of ASTM E1755 and E872, they were all calculated on a dry basis. For both wood species, all tests were preformed in triplicate and the mean values were taken to ensure results accuracy and repeatability.

The experimental TGA apparatus was a thermogravimetric analyzer (STA 449 F3 Jupiter, NETZSCH) with a weighting sensitivity of 0.025 μg and a balance drift lower than 2 μg/hour. The TGA-DCS sample carrier was mounted for simultaneous measurement of mass loss and heat flux. All measurements were carried out under a nitrogen flow of 50

mL/min and a protective gas flow of 20 mL/min. Dynamic tests started by heating the sample up to 100 °C for a 30-minute plateau at this temperature to eliminate the residual water, then the temperature increased to 800 °C with a constant heating rate (10, 5, 2 and 1 K/min). Static tests started by the same plateau at 100 °C, then followed by a heating phase at 10 K/min to the desired temperature (250 °C, 300 °C, 350 °C, 400 °C, 450 °C and 500 °C) for a 2-hour plateau.

Blank experiments were conducted for all experimental protocols and each experiments was repeated three times. In order to exclude buoyancy effects and effect of crucible mass on heat capacity, each final result is the raw data calibrated by subtracting a blank test performed with the same protocol and the same crucible. The mass recorded at the end of 100 °C plateau was considered as oven-dry mass (m_0) for the determination of mass loss. In equation 1, the dimensionless residual mass (DRM) is defined as the ratio of the instantaneous sample mass (m_s) over the oven-dry mass:

$$\mathrm{DRM}(t) = \frac{m_s(t)}{m_0} \tag{1}$$

The dimensionless mass loss (DML, equ. 2) is simply the complement to the unity:

$$\mathrm{DML} = 1 - \mathrm{DRM} \tag{2}$$

3. Modeling

3.1. DAEM formulation

The DAEM formulation (equ. 3, Vand, 1943) assumes that the product degrades through a large number of independent, parallel and irreversible first-order reactions i:

$$\frac{dV_i}{dt} = k_i(V_i^{\infty} - V_i) \tag{3}$$

$$k_i = A_i \exp\big(-\frac{E_i}{RT}\big) \tag{4}$$

In these equations, V_i represents the quantity of volatiles generated during reaction i, V_i^{∞} is the total quantity likely to be produced by this reaction. k_i is the kinetic constant for reaction i. Its thermal activation is assumed to obey an Arrhenius law (equ. 4), defined

by an activation energy E_i and a pre-exponential factor A_i (kinetics constant at infinite temperature).

A time integration of equation (3) allows the time evolution of V_i to be derived as:

$$V_i^\infty - V_i(t) = V_i^\infty \exp\left(-\int_{t_0}^{t} k_i(T(t))dt\right) \tag{5}$$

In practice, a continuous function is used instead of equation (5) to represent a large number of reactions. This function $F(E)$ represents the fraction of volatiles produced by all reactions which have an activation energy smaller than E. The derivative of function F over the activation energy is a distribution function $f(E)$ which represents the potential of volatile production related to each energy value E:

$$dV^\infty = V^\infty f(E)dE \tag{6}$$

Assuming the pre-exponential factor to be the same for all reactions ($A_i = A\ \forall i$), a combination of equations (5) and (6) yields equation (7):

$$1 - \frac{V(t)}{V^\infty} = \int_{-\infty}^{\infty} exp\left(-\int_{t_0}^{t} Ae^{-E/RT(t)}dt\right) f(E)dE \tag{7}$$

Obviously, the whole set (continuous or discrete) of reactions should represent the entire product. Hence the integration over the entire range of activation energy gives the total potential of volatiles (equ. 8) that can be produced by the product:

$$\sum_{i=-\infty}^{+\infty} V_i^\infty = V^\infty \qquad or \qquad \int_{-\infty}^{+\infty} dV^\infty = V^\infty \tag{8}$$

The norm of function f therefore equals the unit (equ. 9):

$$\int_{-\infty}^{+\infty} f(E)dE = 1 \tag{9}$$

3.2. Gaussian distributions

A common practice is to adopt a Gaussian function for this distribution (or a combination of Gaussian functions). Function f is then defined by the average energy E_0 and its standard deviation σ (equ. 10) . The factor $\frac{1}{\sigma\sqrt{2\pi}}$ ensures the unit norm:

$$f(E) = \frac{1}{\sigma\sqrt{2\pi}} \exp\left(-\frac{(E-E_0)^2}{2\sigma^2}\right) \tag{10}$$

In order to use such a function in a computational code, the domain of this function, defined from $-\infty$ to $+\infty$, has to be restricted to a finite interval and, inside this interval, the continuous function should be approximated by a set of discrete values. As a Gaussian function is well defined by its standard deviation σ, it is reasonable to limit its domain over a certain number k of σ : $[E_0 - k\sigma, E_0 + k\sigma]$ and, inside each interval of length σ, approximate the function by m increments dE of equal length, as expressed in equation (11):

$$E_i = E_0 - n\sigma + (i - 0.5)dE, \quad i = 1, 2km$$
$$with \qquad dE = \sigma/m \tag{11}$$

Equation (12) depicts the corresponding discrete weighting factors of the Gaussian distribution:

$$f_i = f(E_i) = \frac{1}{\sigma\sqrt{2\pi}} \exp\big(-\frac{(E_i - E_0)^2}{2\sigma^2}\big) \tag{12}$$

For the discretized function to correctly represent the continuous function, k has to be equal or greater than 3 (with $k = 3$, the area under the curve is 99.7% of the total area, against 95.4% for $k = 2$). Preliminary simulations have shown that a typical m value of 10 allows a precise restitution of the kinetics (Fig. 1).

3.3. Gamma distributions

In the present work, we used gamma distributions as non-symmetrical distributions. The function f is defined by a minimum energy value E_{min} and two independent parameters, for example, the shape parameter α and the rate parameter β:

$$f(E) = Gamma(\frac{E - E_{min}}{E_{min}}, \alpha, \beta)$$
$$where \qquad Gamma(x, \alpha, \beta) = \frac{\beta^\alpha x^{\alpha-1} e^{-x\beta}}{\Gamma(\alpha)} \tag{13}$$

Where Γ is the gamma function defined as $\Gamma(z) = \int_0^\infty x^{z-1}e^{-x}dx, \quad (z > 0)$.

To sample equation (13) for modeling purposes, the domain of the gamma distribution is restricted to a finite interval $[0, x_{max}]$, where x_{max} is n times the expected value (α/β). Function f is therefore approached on the interval $[E_{min}, E_{max}]$, with $E_{max} = E_{min}(1 +$

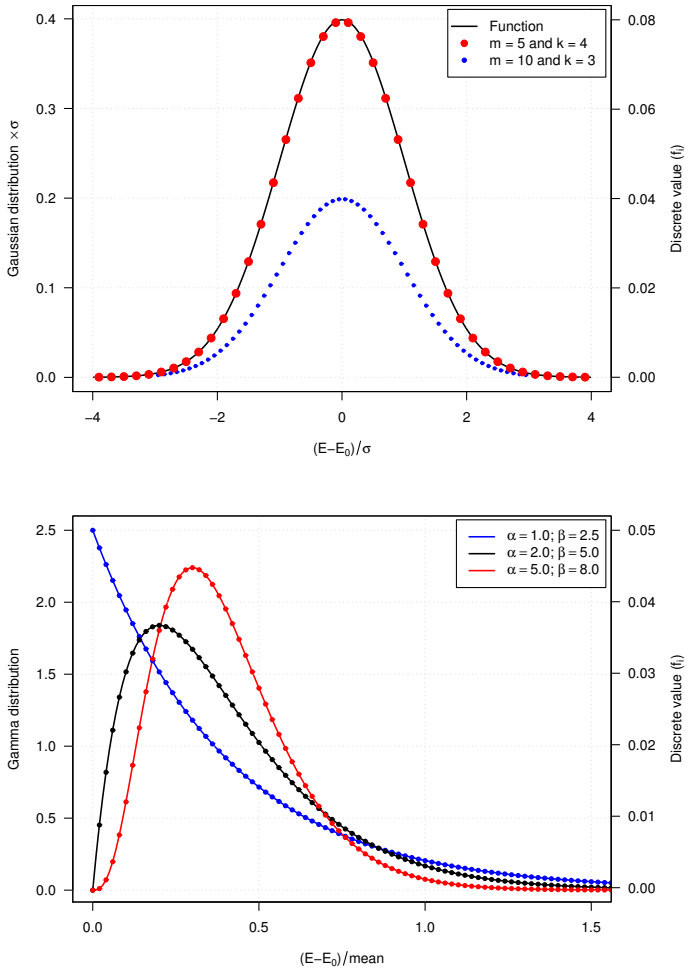

Figure 1: a) Sampling the Gaussian curve to get the discrete values f_i of function f. These values are proportional to the number of points i within each segment of length σ), b) The diversity of shapes that could be obtained with gamma distributions and its sampling obtained using 100 points over the interval $[E_{min}, E_{min}(1 + n\alpha/\beta)]$.

$n\alpha/\beta$). Inside this interval, the function f is discretized in m increments dE of equal length (equ. 14):

$$E_i = E_{min} + (i - 0.5)dE, \quad i = 1, m$$
$$with \qquad dE = (E_{max} - E_{min})/m \tag{14}$$

In this work, the gamma distributions were sampled with $n = 5$ and $m = 100$, which insures an accurate representation of the continuous function.

3.4. Computational implementation

Thanks to this discrete approximation, the kinetics of volatiles production is easily deduced from equation (3). Equations (15) and (16) summarise the set of equation to be computed:

$$\frac{dV}{dt} = \sum_{i=1}^{2km} \frac{dV_i}{dt} = \sum_{i=1}^{2km} k_i(V_i^\infty - V_i(t)) \tag{15}$$

$$k_i = A \exp\big(-\frac{E_i}{RT(t)}\big); \quad V_i^\infty = f_i V^\infty \quad ; \quad V_i(t=0) = 0 \tag{16}$$

In the simulation code, the values of E_i and f_i are computed just once during the initialization procedure. On the contrary, all values of V_i have to be stored and updated along the simulation. Last refinement, the increments update along the time step of the kinetics defined by equation (15) is a first order approximation. However, due to thermal activation, former works (Rousset et al., 2006; Turner et al., 2010) told us that the combination of high temperature level and wide range of activation energy in DAEM might result in very small characteristic times (the factor τ in the time function $exp(-t/\tau)$, i.e. the inverse of k_i in equation 5). To ensure accuracy, an exact formulation of the increment of the chemical reactions during time step dt has been implemented (equ. 17) . This involves an exponential factor in the time increment expression:

$$dV_i = \{1 - exp(-k_i dt)\}(V_i^\infty - V_i(t)) \tag{17}$$

As several distributions are often required to correctly represent the kinetics (we will use three distributions in the present work), equation (15) should be summed over all distributions. As each distribution n has its own sampling, the discrete coefficients should

be indexed by the distribution number (f_i^n). Similarly, the total volatile substances likely to be produced by the distribution n is called $V^{n,\infty}$.

The final formulation for a computational solution of the DAEM model with three distributions is summarized as the change dV^n of total volatiles produced over the time step n, which represents the time interval $[t^n, t^{n+1}]$ with $t^{n+1} = t^n + dt$:

$$dV^n = \sum_{n=1}^{N} \sum_{i=1}^{2km} dV_i^n = \sum_{n}^{N} \sum_{i}^{2km} \{1 - exp(-k_i^n dt)\}(V_i^{n,\infty} - V_i^n(t)) \tag{18}$$

$$k_i^n = A^n \exp\left(-\frac{E_i^n}{RT(t)}\right); \quad V_i^{n,\infty} = f_i^n V^{n,\infty} \quad ; \quad V_i^n(t=0) = 0 \tag{19}$$

$$DML(t^N) = \sum_{n=0}^{N-1} dV^n$$

$$DRM(t^N) = 1 - DML(t^N) \tag{20}$$

The incremental DAEM formulation (equ. 18-20) allows any pathway time-temperature to be simulated. In the following, all simulations will be performed with the actual temperature, as recorded for each test by the TGA device.

3.5. Identification

The distribution parameters were determined by inverse analysis. The identification process minimises the objective function based on the difference between the experimental and calculated DRM values, computed in the sense of the mean-square error over a time interval ranging from the end of the drying plateau (time indice i_{ini}) to the end of the experiment (time indice i_{fin}). Moreover, in order to benefit from all the experimental information, this objective function F_{obj} is computed over several tests simultaneously (the 4 dynamic tests simultaneously in the present work):

$$F_{obj} = \frac{1}{N_{tests}} \sum_{\ell=1}^{N_{tests}} \left[\frac{1}{(i_{fin} - i_{ini} + 1)} \sum_{i=i_{ini}}^{i_{fin}} (\mathrm{DRM}_i^{\ell,exp} - \mathrm{DRM}_i^{\ell,cal})^2 \right] \tag{21}$$

In equation (21), the experimental dimensionless residual mass $DRM_i^{\ell,exp}$ is obtained by equation (1) and the calculated dimensionless residual mass is tied to the DEAM model (equ. 18) through to total, dimensionless, mass of volatiles produced at time t ($\mathrm{DRM}_i^{\ell,cal} = 1 - V^{\ell}(t_i)$).

The kinetic model is solved using an in-house software written in Fortran 95 by Patrick Perré. This code solves equation (18) with the actual furnace temperature of each test, as collected by the TGA device, for each time t_i. The objective function is minimized using the Nelder-Mead algorithm (Nelder and Mead, 1965). As all experiments are treated simultaneously, all experimental conditions are computed for each increment of the Nelder-Mead algorithm, using the current set of parameters, to evaluate the objective function. The computational engine is embedded in a graphical library *Winteracter* to create a Windows application, with fields for parameter input/output and curve plot for visual check. It can be used either to simulate desired configurations or to identified parameters values from a set of experimental data.

It is important to notice that the identification procedure is not straightforward as many local minima exist: the initial parameter guess is therefore important for the algorithm to converge towards the global minimum. The in-house graphical application allows the free parameters, the experimental tests under interest and the active time interval of each test to be chosen. In order to tune the initial guess, we usually proceed stepwise : the first distributions are optimized over a reduced range of temperatures (namely by selecting a subset of the experimental times) and additional distributions are added along with additional experimental information. Finally, all tests are optimized with the full set of parameters to refine the solution. This is restarted several times with a large initial simplex, to check that the solution is the global minimum. The graphical output of the application and the display of residues greatly ease the procedure.

3.6. Enthalpy of reaction

The enthalpies of reaction are of utmost importance at the industrial scale to control thermal runaway and to evaluate the energetic yield over the whole transformation chain of biomass. Consequently, these values need to be included in the enthalpy balance to compute the source/sink terms due to degradation reactions. This is crucial to predict the temperature field, hence the kinetic activation at the scale of one macroscopic particle or at a level of bed of particles (Turner et al., 2010; Perré et al., 2013). Yet, the literature is still sparse in values of reaction enthalpies.

A first sight, the best way to measure enthalpies of reaction is to use isothermal tests, during which the heat capacity of sample and crucible is not involved. However, as pyrolysis reactions are quite slow, the total reaction enthalpies spread over long duration and produce in a very low signal. In such conditions (small heat flux and large durations) the drift of the heat flux baseline turns out to be larger than the signal. Instead, in the present work, we used dynamic tests, together with the robust, validated, DAEM model, to get a quite good accuracy of the identified reactions enthalpies, using the whole piece of information available with a ATG-DSC device : heat flux, temperature and mass loss. It is important to note that such an analysis would not have been possible with a simple DSC which is not able to give the mass evolution, in spite of the much better accuracy of such devices regarding heat flux.

To that purpose, the energy balance should to be properly formulated (equ. 22). In particular, the change of mass over time needs to be considered to evaluate the heat required to change the sample temperature. As the transformation occurs at constant pressure, we write the enthalpy conservation of the system (sample + crucible) between time t and time $t + dt$.

$$\underbrace{m_c h_s + m_s h_s}_{\text{Time } t} = \underbrace{\dot{Q}dt + \dot{S}dt + m_c(h_s + dh_c) + (m_s - dm)(h_s + dh_s) + dmh_v}_{\text{Time } t+dt} \tag{22}$$

Where h are the specific enthalpies, $\dot{Q}$ the heat flux provided to the system, $\dot{S}$ the source term due to chemical reactions and dm the quantity of volatiles formed during the time interval dt. Indices c, s and v stand for crucible, sample and volatiles respectively.

Rearranging equation (22) in terms of derivatives truncated at the first order yields equation (23):

$$-\dot{Q} = m_c \frac{dh_c}{dt} + m_s \frac{dh_s}{dt} + \dot{S} + \frac{dm}{dt}(h_v - h_s) \tag{23}$$

The fourth term of the right-hand side of equation (23) represents the enthalpy of volatilisation (Frederick Jr and Mentzer, 1975; Suwardie and Artiaga, 2000). In the following, the two last terms of the right-hand side are considered lumped together to form the production of pyrolysis enthalpy $\dot{H}_{pyro}$. As the blank tests are performed with the

same crucible, the thermal inertia of the crucible is canceled after blank correction. The final equation for the blank corrected test is obtained by introducing the heat capacity of the sample (equ. 24):

$$-\dot{Q} = m_s(t)c_{p,s}\frac{dT}{dt} + \dot{H}_{pyro} \tag{24}$$

In the result section, the pyrolysis enthalpy $\dot{H}_{pyro}$ will be identified for the predicted heat flux (right-hand side of equation 24 : sum of enthalpy production and sensible heat) to match the heat flux measured by the TGA-DSC device ($-\dot{Q}$). In this calculation, we will assume that the reaction enthalpy, ΔH^n, is the same for all reactions involved in a given distribution n. This is a quite strong assumption, but was required for the identification to be realistic. The enthalpy production (equ. 25) reads then as follows:

$$\dot{H}_{pyro} = \sum_{n=1}^{N}\sum_{i=1}^{2km}\Delta H^n\frac{dV_i^n}{dt} \tag{25}$$

Keeping in mind that $V(t)$ is the dimensionless production of enthalpy, the final equation (equ. 26) used in the identification becomes:

$$-\dot{Q} = m_0(1-V(t))c_{p,s}\frac{dT}{dt} + \sum_{n=1}^{N}\Delta H^n\left(\sum_{i=1}^{2km}k_i^n(V_i^{n,\infty}-V_i^n(t))\right) \tag{26}$$

4. Identification and validation

4.1. Identification of DAEM parameters

Dynamic experiments were used to identify the parameters of the DAEM model. It is important to remind here that the four dynamic tests were used simultaneously (equ. 21) for each species. The importance of this feature was reported in Soria-Verdugo et al. (2015). Note however that our learning database includes a wider range of heating rates (from 1 to 10 K/min) than in this reference. For a Gaussian distribution, E_0 is the mean activation energy, which informs on the global resilience to decomposition: pseudo-components with smaller value of E_0 are prone to decompose more easily than those with high E_0. The standard deviation of the Gaussian distribution σ quantifies the width of activation energy values around the mean value. A distribution with a large standard

deviation means that the corresponding pseudo-component decomposes over a large temperature range (or a large range of characteristic times) around the average value. The pre-exponential factor A controls the overall reaction rates. The weighting factor $V^{n,\infty}$ represents the total proportion of the initial biomass that can produce volatiles.

315

During the identification procedure, several distributions were required to correctly represent the evolution of DRM over the whole range of experimental conditions. As our strategy was to limit the number of degrees of freedom, we tried to limit the number of distributions. Two Gaussian distributions were able to capture the behaviors for moderate
320 temperature levels. However, the symmetry of Gaussian functions is a strong constraint regarding the behaviour of thermo-activation: with a symmetrical distribution, it is not possible to spread the kinetics over high temperature levels without spreading also the kinetics over low temperatures. This fact was already observed and led scientists to use non-symmetrical distributions (Cai et al., 2014; Li et al., 2019). The third distribution,
325 devoted to the behavior up to 800 °C, was therefore set as a gamma distribution. This choice was crucial to obtain a good representation with three distributions. During the optimisation procedure, the need of asymmetry for this third distribution was so strong that the minimum value of residues was obtained with a value of α less than one, with induces an infinite value at zero. Such a function becomes very tricky to represent by
330 discrete values : the parameters values depend on the sampling density, which is very difficult to reproduce. To avoid this side effect, we added the constraint $\alpha \geqslant 1$. The inverse procedure eventually gives $\alpha = 1$, which limits the gamma distribution to the subset of exponential functions and reduced by one the degrees of freedom.

As the learning database includes the asymptotic behavior (temperature level and
335 duration enough to approach equilibrium), the sum of the weighting factors of all distributions is smaller than the unit. The complement of this sum to the unity therefore represents the asymptotic value of Dimensionless Residual Mass at infinite time.

In spite of slight differences, the parameters values identified for spruce and poplar depict the same trends (Table 1). In both cases, the second distribution has the largest
340 weighting factor, indicating the largest portion of pseudo-components described by this

distribution. For both species, the standard deviation of the second distribution is very small. No kinetics difference was observed for $\sigma \to 0$. This results in a unique activation energy, 183.3 kJ/mol for spruce and 181.4 kJ/mol for poplar, in good agreement with the value 185 kJ/mol obtained in Sonobe and Worasuwannarak (2008). The second distribution is basically reduced to a simple first-order reaction (a Dirac distribution), which decreases the number of degrees of freedom by one. This is explained by the sudden and large mass loss arising at around 300 °C. Finally, the third distribution acts after the second one in terms of temperature level and its action lasts over a large range of high temperatures. Finally, the proposed DAEM model comprises three different distributions:

- a Gaussian distribution for hemicelluloses,
- a Gaussian function degenerated into a Dirac function for cellulose,
- a gamma function degenerated into an exponential function for lignins.

Table 1: DAEM parameters of spruce and poplar identified on dynamic pyrolysis experiments. Parameters in red represent meaningless parameters related to the degeneration of distribution functions (Gaussian to Dirac and gamma to exponential).

Biomass	Distribution	V_{max}	E_0 $(kJ \cdot mol^{-1})$	σ, α or β $(kJ \cdot mol^{-1}, -, -)$	A (s^{-1})
Spruce	1 (Gaussian)	0.2344	168.5	$\sigma = 7.51$	9.67×10^{12}
	2 (Gaussian)	0.4927	183.3	$\sigma = 0.089$	
	3 (gamma)	0.1563	182.8	$\beta = 2.812; \alpha = 1$	
Poplar	1 (Gaussian)	0.2584	163.6	$\sigma = 6.62$	7.03×10^{12}
	2 (Gaussian)	0.4928	181.4	$\sigma = 0.128$	
	3 (gamma)	0.1630	181.3	$\beta = 2.205; \alpha = 1$	

For both species, the 3-distribution DAEM model is in excellent agreement with the experimental results (Fig. 2). This proves the ability of model to describe the pyrolysis behavior over a large range of temperatures and heating rates although we were frugal in the number of independent parameters. This qualitative assessment is confirmed by

objective criteria (Table 2). The standard deviation is around or less than 0.5% and the maximum deviation, a very severe criterion, is around 1 to 1.5 %, except for spruce at 10 °C per minute, for which a slightly larger difference (2.27%) is observed at the end of the test. This difference is not obvious on the graph as the maximum deviation is obtained during the rapid mass decrease, where the curve slopes are very large. These excellent results are obtained by assuming a constant pre-exponential factor A, identical for all distributions ($\forall n, A^n = A$). This is in contradiction with the latest published works in which authors propose the pre-exponential factor to be a function of temperature, heating rate or average activation energy (Cai and Liu, 2008; Sonobe and Worasuwannarak, 2008; Sfakiotakis and Vamvuka, 2015; Czajka et al., 2016; Xu et al., 2018). Even with our experimental datasets that include a large range of temperature levels and residence times, it was not necessary to use such functions, neither to obtain a small residues nor to successfully validate the mode against distinct time-temperature pathways. We can therefore affirm that a constant value of A is perfectly able to reproduce the kinetics behavior over a wide range of temperature levels and heating rates. We owe this success to the strategy to identify one single set of parameters simultaneously on the entire series of tests, together with the highly asymmetrical shape of the third distribution.

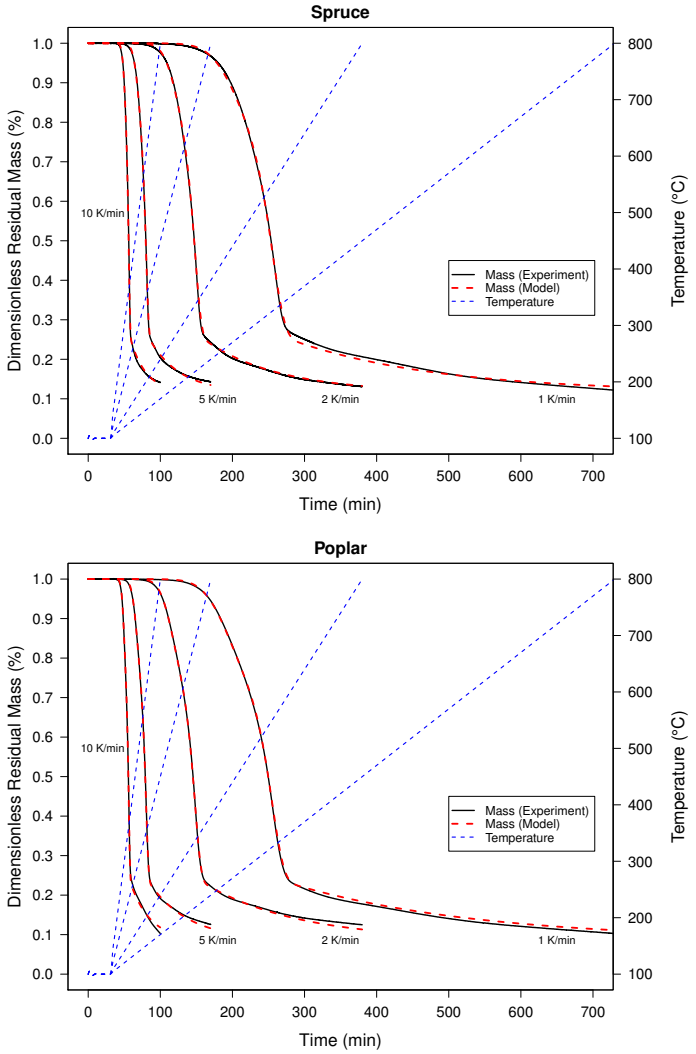

Figure 2: TG curves for dynamic experiments at different heating rates (10 K/min, 5 K/min, 2 K/min and 1 K/min) and corresponding DAEM curves based on identified parameters and temperature evolutions. Time origin is at the end of the 30-minute 100°C plateau.

The temperature response of the three distributions together with these respective weighting factors confirm well-accepted trends in the pyrolysis behavior of lignocelluloses (Chen et al., 2015; Cordero et al., 1990). The first distribution accounts for the degradation of hemicelluloses, the most prone to thermal degradation. Hemicelluloses are linear branched polymers made by different types of monosaccharide units (Xu et al., 2013) and it decomposes in the range 225-325°C. Poplar hemicelluloses are mainly composed of

xylan, whereas spruce hemicellulose are mainly composed of glucomannan(Wang et al., 2017b). In agreement with published results (Prins et al., 2006; Cavagnol et al., 2013), this explains that spruce is more thermally stable than poplar at moderate temperatures: E_0 of the first distribution is smaller for poplar than for spruce.

As can be seen from the V_{max} values, the second distribution affects roughly half of the production of volatile substances with rapid degradation above 300 °C. This is undoubtedly the signature of cellulose, which represents ca. 50% of the total mass and is very resilient to degradation in crystalline state, but with a rapid thermal decomposition once melt (Lv et al., 2015). Cellulose has macromolecular structures which are constructed by semi-crystalline array of $\beta-1,4$ glucan chains and it decomposes at 325-385°C (Chen and Kuo, 2010; Shafizadeh, 1985). For Gaussian distributions 1 and 2, the present results depict similar trends as those proposed by Chen et al. (2016). However, our third distribution is very different from the very wide Gaussian distribution proposed in (Chen et al., 2016) : the gamma distribution captures nicely the degradation of the most reluctant part of the biomass, which can be attributed mostly to lignins (Poletto et al., 2012). Lignins present a highly branched three-dimensional phenolic structure made of C_6C_3 units, namely, p-hydroxyphenyl (H), guaiacyl (G), and syringyl (S) units, in various proportions depending on the species. Lignins present a large range of decomposition temperature from 250 °C to over 500 °C. Hardwood lignins are composed of S and G units, together with trace amounts of H units. Softwood lignins consist mainly of G units and low levels of H units (Boerjan et al., 2003; Whetten et al., 1998). Consequently, spruce lignins contain fewer β-O-4 bonds and more 5-5 branching structures than poplar lignins. As β-O-4 bonds are the main targets of thermal degradation (Rousset et al., 2009; Assor et al., 2009), it is not surprising to obtain a minimum activation energy E_0 for the gamma distribution slightly smaller for poplar.

As a summary, hemicelluloses are the first components to be altered by temperature, cellulose, ca. half the cell wall mass, is very resilient before melting, but depicts a rapid degradation after melting (with a melting temperature around 300 °C) and lignins is the part of the cell wall the most resilient to degrade. This simple correspondence between the distributions and the components of the cell wall is certainly related to the absence of

significant interaction between these components during pysolysis (Navarro et al., 2009; Cavagnol et al., 2013).

Table 2: Learning procedure on dynamic tests : quality of the model with the best fit of parameters for each temperature level assessed as the standard deviation and the maximum error.

	Heating rate (K/min)	Standard deviation (% DRM)	Maximum deviation (% DRM)
Spruce	10	0.45	2.27
	5	0.43	1.22
	2	0.35	1.57
	1	0.58	1.56
Poplar	10	0.53	1.43
	5	0.43	1.09
	2	0.55	1.31
	1	0.50	1.00

4.2. Validation on static experiments

So far, we proved the ability of the kinetic model to represent a quite large pyrolysis database with a moderate number of identified parameters. In this section, the model will be tested on a completely different experimental database, the set of static tests. The experimental and predicted DRM curves are depicted in figure 3. It is worth mentioning that this is a true validation test : the parameters used in the model are the parameters derived from the dynamic tests of Table 1, without any further identification.

Overall, the predictions are in very good agreement, even with the static tests at moderate temperature (250 °C, 300 °C). These tests are severe due to their slow kinetics, without asymptotic behavior. Such good predictions obtained for this demanding validation confirm the resilience of the DAEM formulation in comparison with a set of simple chemical reactions occurring simultaneously or in cascade (Rousset et al., 2006; Cavagnol et al., 2015). The good agreement is confirmed by the computed residues (Table 3). This is an additional proof regarding the assumption of constant and common value for the

pre-exponential factor A.

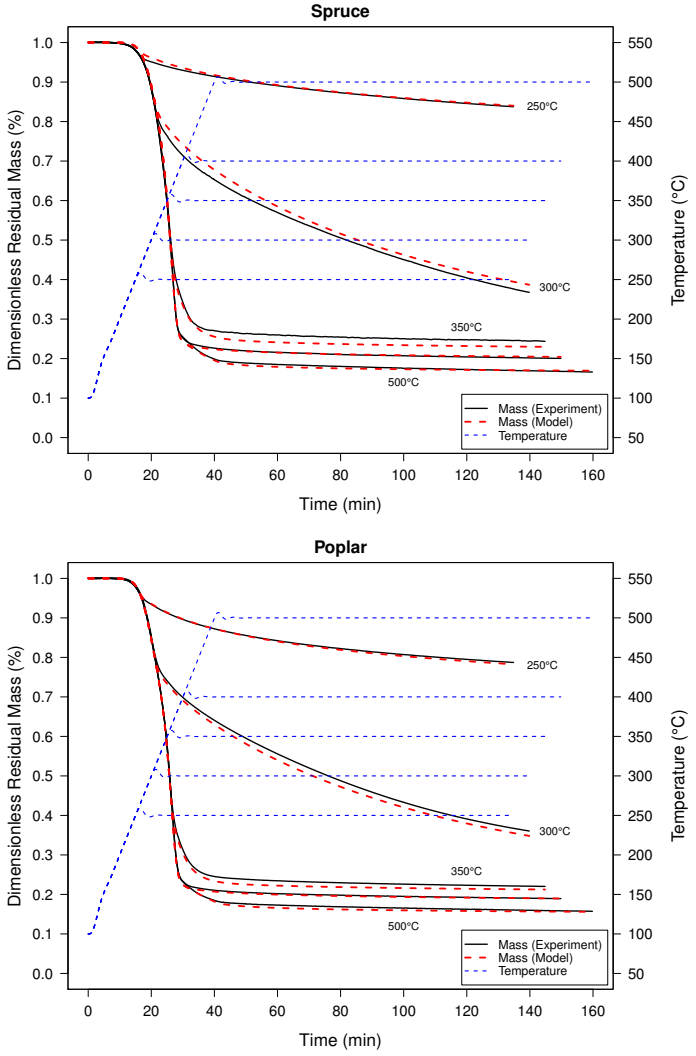

Figure 3: Model validation using a set of static experiments at different plateau temperatures (250 °C, 300 °C, 350 °C, 400 °C and 500 °C).

Table 3: Validation step on static tests : quality of prediction with the parameters fitted on the learning database for each plateau temperature assessed as the standard deviation and the maximum error.

	Temperature (°C)	Standard deviation (% DRM)	Maximum deviation (% DRM)
Spruce	250	0.39	1.22
	300	1.62	2.87
	350	1.48	1.92
	400	0.42	2.14
	450	0.44	2.18
	500	0.51	2.17
Poplar	250	0.32	0.53
	300	1.21	1.64
	350	0.96	1.33
	400	0.33	1.66
	450	0.83	1.93
	500	0.55	1.49

The rate of decomposition, the first derivative of the differential thermogravimetry (DTG) curves, depicts more detail during the decomposition process as it is more affected by slight changes during the reactions. Comparing experiment and model prediction in terms of derivative is very challenging as it is likely to reveal any differences between the curves. For the sake of example, the results obtained for poplar are shown in figure 4. One might observe that the experimental derivative is noisy, which is a classical effect when deriving an experimental curve. Yet, the DAEM model perfectly predicts the degradation rate, both in terms of position and intensity, over the wide range of temperatures of these static tests. This is an additional and convincing proof of validation. The test at 250 °C depicts a very small DTG peak at 20 hours, due to the partial degradation of hemicelluloses occurring at this temperature level. The peak significantly increases at 300 °C and spreads over slightly longer times. For tests at 350 °C, the shape clearly depicts a double peak by

its shoulder on the left side due to the degradation of hemicelluloses followed, at around 350 °C, by the deep and narrow peak formed by the sudden degradation of cellulose. As the degradation of these two components is almost complete at 350 °C, the shape and maximum amplitude are no longer affected at higher temperature values.

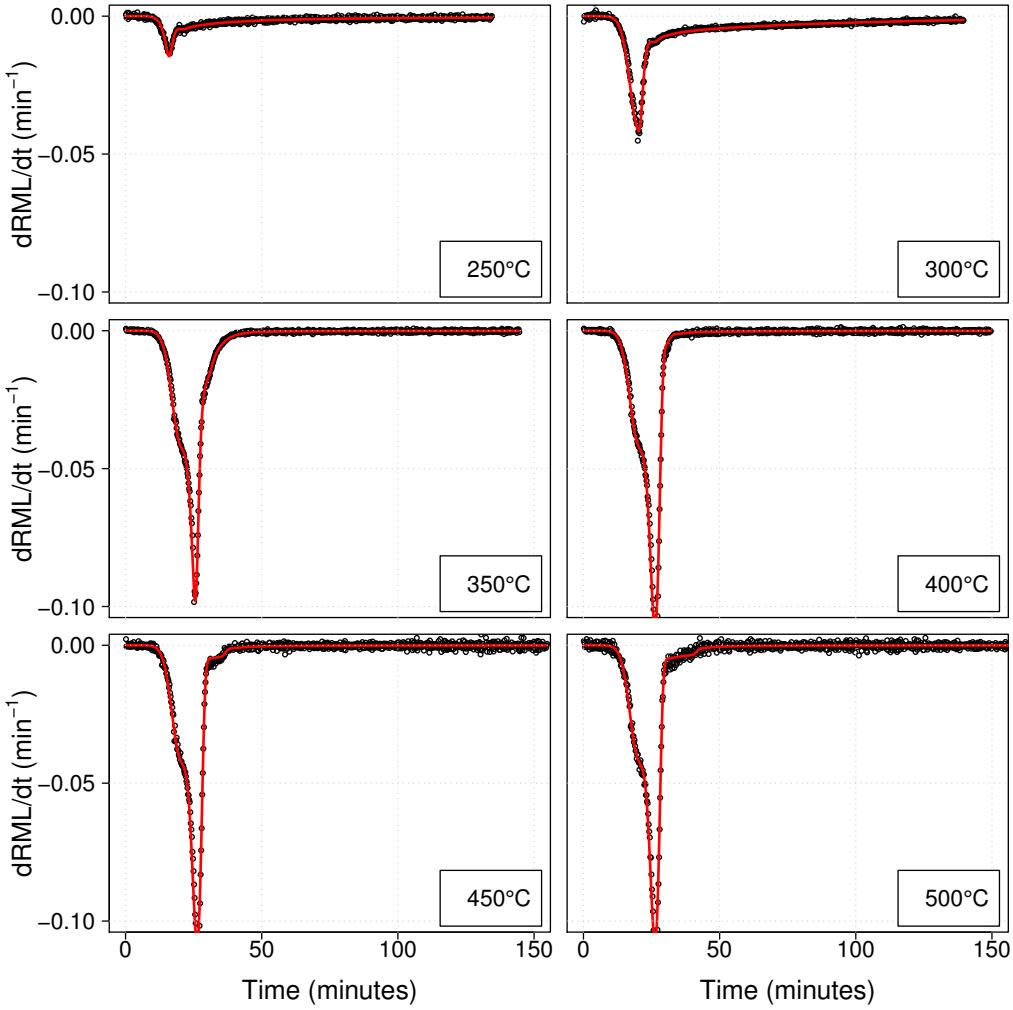

Figure 4: Model validation : experimental (black circles) and corresponding simulation (red lines) of the derivative of DML for the set of static tests Case of poplar.

4.3. Reaction enthalpies

The DSC signal of two types of wood have been analysed to determine the reaction enthalpies. In order to reduce the problem of baseline drift and thanks to the confidence

in the DAEM model provided by the validation step, the dynamic tests at 5 K/min were used to identified the reaction enthalpies using the formulation presented in section 3.4 (equ. 26). The test at 10 K/min was likely to present an even lower baseline shift, but has been discarded due to its noise level.

Figure 5 shows the experimental DSC signal for spruce and poplar as red lines. The model prediction, as computed using equation (26) and after parameter indetification, appears in these figures as blue dashed lines. Note that positive DSC values represent an exothermic behavior (heat removed from the sample) and negative values an endothermic behavior (heat provided to the sample).

During the drying period (plateau at $100°C$), the heat flux needed to water evaporation appears on the experimental curve. This is not present in the model as evaporation is not included in equation 26. At the end of this plateau, the temperature is constant and evaporation stops : consistently, the experimental and simulated heat fluxes are equal to zero. After this plateau, the temperature increases linearly in time, which required the sensible heat to be supplied to the sample. The experimental overshoot is due to the control of the furnace temperature. It can be nicely reproduced by the model as the actual furnace temperature is included in equation (26). While the temperature remains low, no thermal degradations occur : this range is suitable for the determination of the heat capacity. A first exothermic effect can be observed for both species between 60 and 70 minutes (which correspond to the temperature range 250 °C to 300 °C). This peak can be captured by the reaction enthalpy of the first distribution. It is probably due to the charing reaction of hemicellulose, as solid char forms during the primary decomposition at 200-400 °C (Kan et al., 2016; Yang et al., 2007). At 80 minutes (ca. 350 °C) an important endothermic peak is evidenced. This corresponds to the rapid and important mass loss observed during this period. This large endothermic peak is tied to the decomposition of cellulose, which has the highest percentage in biomass and has endothermic pyrolysis characteristic, at this temperature most portion of cellulose decomposes. Afterward, the decomposition of lignin together with secondary reactions including charring and aromatization result in the last and important exothermic peak of the DSC curves (Kifani-Sahban et al., 1997; Haykiri-Acma et al., 2010). To some extent, the decomposition and phase transformations

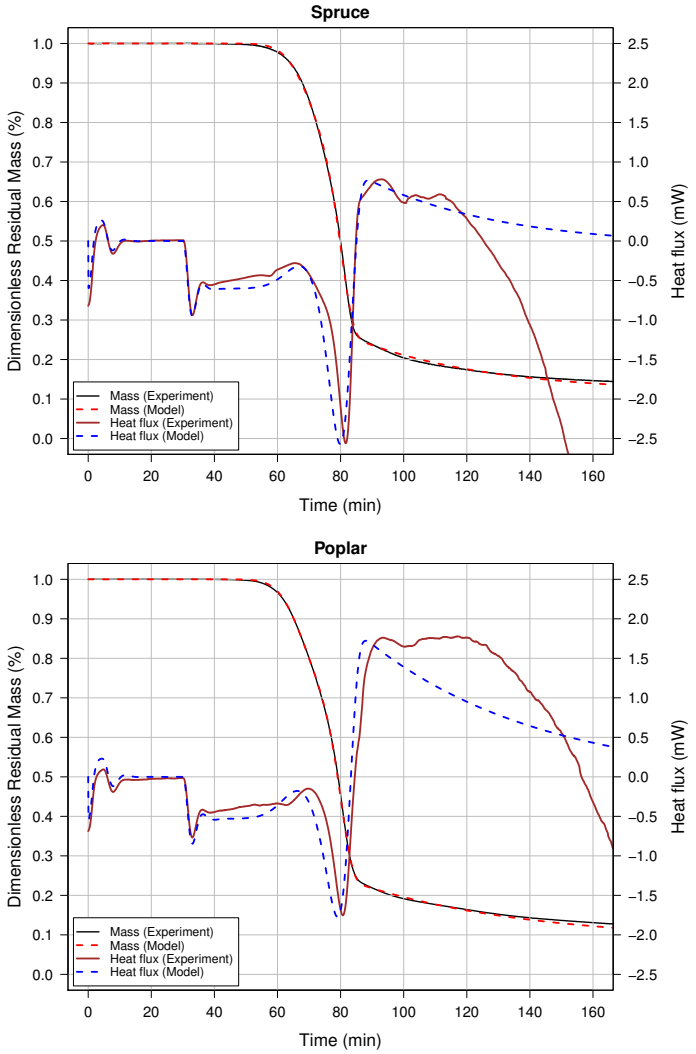

Figure 5: Using the experimental DSC curves to determine reaction enthalpies of spruce and poplar using the dynamic experiments at 5 K/min.

of inorganic matters in ash might also be involved (Vassilev et al., 2013; Febrero et al., 2014).

The difference peaks and troughs of the DSC curves found in our measurements are in good agreement with the analysis performed on the different components of wood (Chen and Kuo, 2011). The enthalpy values determined for both spruce and poplar are summarised in table 4. The identified heat capacity is similar for spruce and poplar. These values are a bit low compared to published values (Guo et al., 2013). Prior to the tests, the device was calibrated using sapphire as reference material and, up to 873 K, the values were in a ±5% agreement with published data (Ditmars et al., 1982). A slight production of heat by thermal degradation is likely to explain the obtained values.

The heats of reaction related to the first Gaussian distribution are slightly exothermic. They allows the first heat flux increase at the beginning of mass loss to be obtained (-140 and -120 kJ/kg for spruce and poplar, respectively). The values obtained for the second Gaussian distribution are definitely endothermic (+339 and +338 kJ/kg for spruce and poplar, respectively). These values were needed to explain the deep decrease of the heat flux during the phase of rapid mass loss, tied to the degradation of cellulose. Finally, very large exothermic values are needed for the third distribution to explain the spectacular increase of heat flux just after the trough of the curve. This heat production should be obtained with a very limited additional mass loss, which explains the high value as the unit for the enthalpy of reaction is in kJ per kg. Note that these values are in agreement with the values obtained by Rath et al. (2003) in the reaction branch producing char and gas. Contrary to all other data that were similar for spruce and poplar, this third reaction enthalpy has a much higher absolute value for poplar (-4300 kJ/kg to be compared to -1900 kJ/kg for spruce). This is consistent with the peak of the heat flux values, much larger for poplar than for spruce. The same trends were observed for all tests, whatever the heating rate (not show here).

At the highest temperature levels, the predicted curves differs from the experimental curves. This is likely to be due to the change of radiative properties between the empty crucible and the crucible with the degraded sample (Rath et al., 2003). To address this problem, we performed tests with a lid, but, as the presence of a lid changes the mass loss,

the DAEM model was not valid any more.

Table 4: Enthalpy for decomposition reactions obtained for spruce and poplar by adjustment on the 5 K/min dynamic tests. Positive value indicates endothermic reaction, and negative value exothermic reaction.

Biomass	$C_p(J/(kg \cdot K))$	$\Delta H^1(kJ/kg)$	$\Delta H^2(kJ/kg)$	$\Delta H^3(kJ/kg)$
Spruce	720	-140	$+339$	-1900
Poplar	650	-120	$+308$	-4300

5. Use of the model

In the previous section, the DAEM parameters has been identified on the learning database. The proposed choice of distributions required only 9 independent parameters : 3 activation energy $E_0(n)$, 3 weighting factor $V^{n,\infty}$, 1 standard deviation $\sigma(1)$, β and the pre-exponential factor A. The DAEM model was then successfully validated using very different temperature-time routes. Thanks to this success, the model was be further used to determine the enthalpies of reaction. In this section, the model is used for prediction purposes : prediction of the pathway in the Van Krevelen's diagram and the control of the temperature rise to limit the released energy.

5.1. Elemental analysis

The results of ultimate and proximate analysis for untreated spruce and poplar are summarized in table 5. The nitrogen content was lower than 0.1% for native samples and lower than 0.3% for treated samples. Sulphur was not detected in any sample. These values are, at best, of the order of the experimental accuracy and were therefore not reported in this table.

Table 5: Ultimate and proximate analysis of native spruce and poplar.

Biomass type	Proximate analysis (wt.%)			Ultimate analysis (wt.%)		
	VM	Ash	FC	C	H	O
Spruce	84.93	0.29	14.77	47.07	5.97	43.65
Poplar	86.29	0.37	13.34	48.06	5.95	43.76

The remaining biomass char of each static test has been collected to determine char yield and to perform elemental analysis (Table 6). For both spruce and poplar the H/C and O/C ratios decrease simultaneously, indicating a pathway towards pure carbon. This is a classical finding in heat treatment of biomass : H and O contents decrease due to the volatilization of organic components into gas with low molecular mass. Figure 6 plots the O/C and H/C ratios found for the different plateau temperatures in a Van Krevelen's diagram (McKendry, 2002). At increasing temperature levels, the positions of char in this diagram move towards the down-left corner which represents highly carbonized material. The difference between spruce and poplar observed at low temperature is not visible on this diagram. On the contrary, char from poplar stands beneath that of spruce for the most severe conditions, indicating that poplar has more prone to charring than spruce for severe pyrolysis.

The difference between the two species is however quite low when plotted as a function of Dimensionless Mass Loss (DML). This allowed us to propose a single set of equations fitted to predict the O/C and H/C ratios as a function of DML:

$$\begin{aligned} O/C &= 1.134 - 0.219 \times exp(1.815 \text{ DML}) \\ H/C &= 0.1534 - 0.0268 \times exp(1.783 \text{ DML}) \end{aligned} \tag{27}$$

Obviously, for prediction purpose, the DML value can be predicted by the validated DAEM model for any time-temperature pathway using equations 18-20.

Table 6: Char yield and ultimate analysis of pyrolysis char from spruce and poplar powder in static tests

	Temperature(°C)	C (wt.%)	H (wt.%)	O (wt.%)	Char yield (wt.%)
Spruce	250	50.77	5.7	39.69	76.67
	300	65.26	4.27	24.53	27.87
	350	71.01	3.09	19.19	24.70
	400	74.28	3.05	15.24	21.54
	450	79.22	3.11	12.42	19.45
	500	82.67	2.88	9.49	17.42
Poplar	250	50.30	5.65	40.1	76.55
	300	62.28	4.75	28.32	32.94
	350	70.90	3.23	19.99	21.57
	400	74.44	2.86	16.44	18.94
	450	77.11	2.87	13.21	16.91
	500	81.50	2.63	9.62	15.73

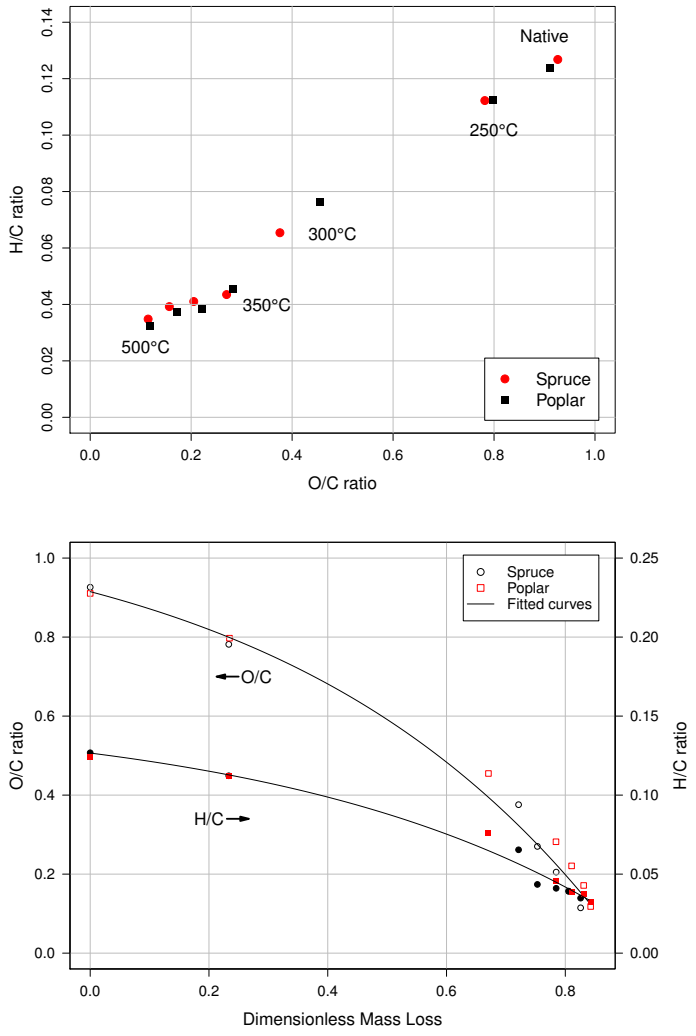

Figure 6: a) O/C and H/C ratios from char of spruce powder and poplar powder and corresponding biomass, b) O/C (open markers) and H/C (plain markers) ratios as a function of dimensionless mass loss (DML). Experimental data and fitted curves.

5.2. Process control

All the kinetic parameters as well as the reaction enthalpies confer a predictive potential to the code. Its eventual purpose is to be implemented in a multi-scale macroscopic particle model, able to deal with the non-uniform variable fields within the particle (Turner et al., 2010) or with a packed-bed (Perré et al., 2013; Perre, 2019). Such a work is in progress in our team. Even at the micro-particle scale, the prediction potential of the model

can be tested. For example, limiting the heat flux due to reactions might be important to minimize the temperature perturbation during ATG tests. Figure 7 compared two different temperature pathway :

1. A linear temperature increase from 100 °C to 650 °C in 200 minutes
2. An optimised control : the temperature increase is controlled to limit the heat flux in the range $[-0.5mW, +0.5mW]$ for a sample of $10mg$ as initial mass.

For case 2), a simple PD (proportional, derivative) control was implemented, which explains the small oscillations. However, it is obvious that the obtained temperature increase allows the same temperature range to be investigated over the experiment duration (200 minutes), while avoiding the heat flux peaks. One can see that the constraint reduces the temperature increase when the kinetics produces high values of heat flux. In order to give an in-depth view of the DAEM model, we plotted the evolution of the three distribution in the case of the optimised control (Fig. 7). The first Gaussian distribution is wide with low activation energy. Consequently, this is the first one to be affected by heat. It gradually disappears, starting to the left-hand side, which represents the lowest activation energies. This peak completely disappears after ca; 50 minutes. The second peak is very narrow and no difference of kinetics may be observed over the, very small, distribution energy. Following the rapid mass loss depicted by all the previous curves, its degradation lasts over a short time interval and disappears completely very soon after the first distribution. Finally, the last distribution is non-symmetrical and depicts a very wide range of activation energies. Again, the kinetics affects the left-hand side of the distribution. After 200 minutes, most of the large values from the left-hand sides disappeared (one has to remember that the initial shape is an exponential curve). However, the right-hand side, which contains very large values of activation energy (above 200 kJ/mol) are not degraded yet. This is consistent with the lignin behaviour, whose degradation spreads over a very large temperature range.

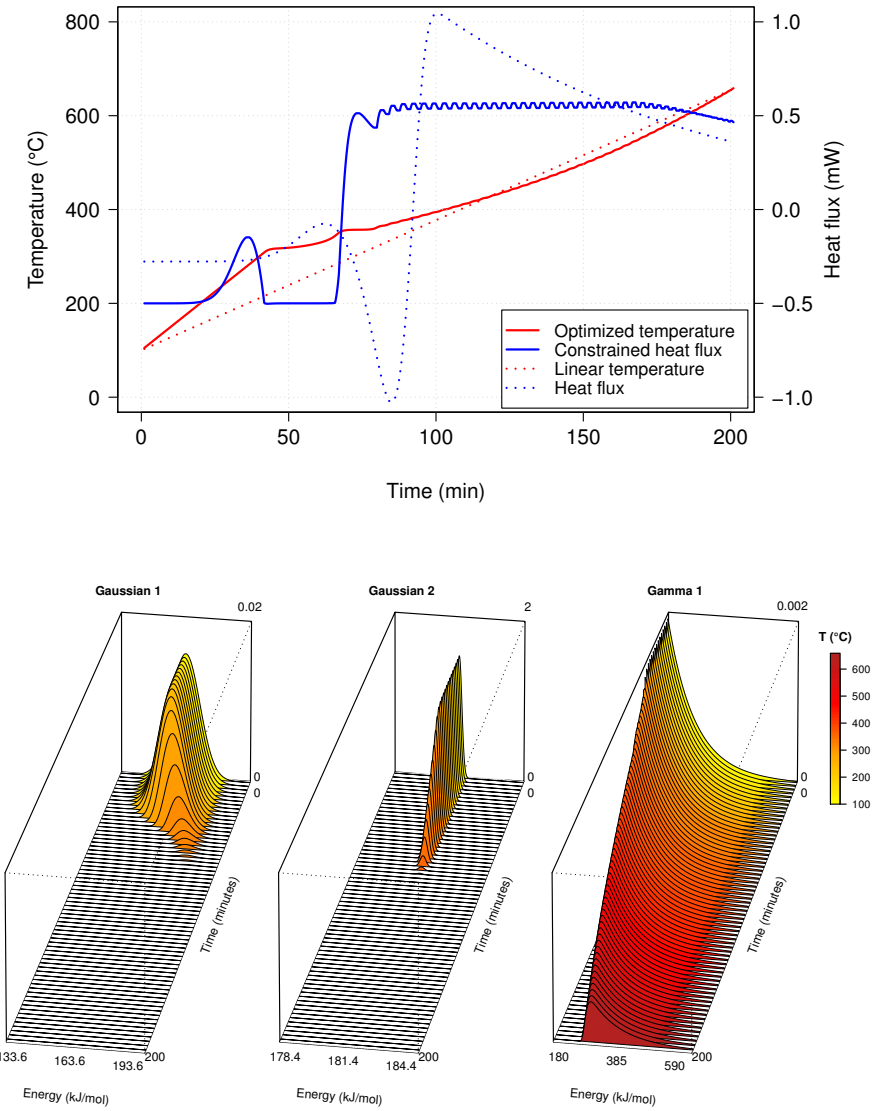

Figure 7: Top), Temperature and heat flux evolution for a constant heating rate and for an optimised temperature profile. Bottom) Evolution of the residual parts of each distribution for the optimised temperature profile.

6. Conclusion

A robust three-distribution DAEM model was derived to simulate two types of lignocellulosic products over a wide range of treatment time and temperatures. The comprehensive approach includes i) parameters identification using a learning database (dynamic tests with different heating rates), validation with static tests ranging from 250 °C to 500 °C and iii) the use of the measured heat flux to determine the heats of reaction. The potential of the model has been highlighted by two application examples : the prediction of the biomass pathway in the Van Krevelen's diagram and the use of the heats of reaction to control the process at the micro-particle level. The main outcomes of this work are as follows :

- The kinetics and heat flux formulation are presented in detail, as well as the computational strategy to correctly solve these equations, which is intended to serve as a guide for the reader,
- To use of a gamma distribution allows the model to include only 9 independent parameters,
- In spite of its sparcity, the model perfectly predicts the kinetics over a large range of temperature and duration, for dynamic and static tests
- Heats of reactions were determined using the experimental DSC signal
- The model has a great prediction potential, including as local model to be included in a multiscale approach

In the near future, this reaction model will be embedded in a comprehensive heat and mass transfer computational code to model the process at the level of a large particle or of a packed-bed of particles. One specific point to be addressed is the crucial question of thermal runaway. Such simulations will be compared to experimental results to check whether or not the heats of reaction identified on powders, with or without lid, remain pertinent for large particles. To the best of our knowledge, this is still an open question that deserves consideration.

Acknowledgement

Financial supports from Grand Reims, the Marne department and the Grand Est region are gratefully acknowledged. Yong Tian acknowledges the financial support by the China Scholarship Council (CSC) for the opportunity to study in France.

CRediT author statement

PP : Conceptualization, Methodology, Formal analysis, Software, Visualization, Writing-Original draft preparation, Writing - Review and Editing, Supervision, Funding acquisition. YT: Investigation, Methodology, Validation, Writing- Reviewing and Editing, Data curation. PL: Methodology, Validation, Writing- Reviewing and Editing, Data curation. BM: Investigation, Validation, Writing- Reviewing and Editing. JEN: Investigation. JC: Resources, Writing- Reviewing and Editing, Supervision, Funding acquisition.

7. Notations

The notations are summarized in tables (7 to 9)

References

Almeida, G., Brito, J.O., Perré, P., 2010. Alterations in energy properties of eucalyptus wood and bark subjected to torrefaction: the potential of mass loss as a synthetic indicator. Bioresource technology 101, 9778–9784.

Alves, S., Figueiredo, J., 1989. Kinetics of cellulose pyrolysis modelled by three consecutive first-order reactions. Journal of Analytical and Applied Pyrolysis 17, 37–46.

And, D.E.D., Brown, R.C., 2003. Enthalpy for pyrolysis for several types of biomass. Energy and Fuels 17, 934–939.

Antal, M.J., Varhegyi, G., Jakab, E., 1998. Cellulose pyrolysis kinetics: revisited. Industrial and Engineering Chemistry Research 37, 1267–1275.

Table 7: List symbols (Latin letters)

Symbol	**Name**	**Unit**
A	pre-exponential factor	s^{-1}
c_p	specific heat capacity at constant pressure	$J.kg^{-1}.K^{-1}$
DRM	Dimensionless Residual Mass	-
DRL	Dimensionless Mass Loss	-
f	distribution function	J^{-1}
k	kinetics constant	s^{-1}
h	specific enthalpy	$J.kg^{-1}$
$\dot{H}_{pyro}$	production of pyrolysis enthalpy	J^{-1}
E	activation energy	J
E_0	Reference energy of a distribution	J
$\boldsymbol{j}_k$	diffusive flux of component k	$kg.m^{-2}; s^{-1}$
$\boldsymbol{J}_q$	heat flux	$W.m^{-2}$
m	mass	kg
M	molar mass	$kg.mole^{-1}$
P	pressure	Pa
$\dot{Q}$	heat flux	J^{-1}
R	gas constant	$J.kg^{-1}.K^{-1}$
$\dot{S}$	heat source due to reactions	J^{-1}
T	temperature	K or $^{\circ}C$
V	volatiles produced by a reaction	kg

Table 8: List of symbols (Greek letters)

Symbol	**Name**	**Unit**
α	shape parameter of the gamma distribution	-
β	rate parameter of the gamma distribution	-
ΔH	reaction enthalpy of a distribution	J
λ	thermal conductivity	$W.m^{-1}.K^{-1}$
Γ	Gamma function	-
μ	dynamic viscosity	$kg.m^{-1}.s^{-1}$
ρ	density	$kg.m^{-3}$
σ	standard deviation	J^{-1}
τ	time constant	s

Table 9: Subscripts and superscripts

Subscripts	**Meaning**
b	bound water
c	crucible
v	volatiles
Superscript	**Meaning**
n	relative to distribution n
∞	total potential production of volatiles

Assor, C., Placet, V., Chabbert, B., Habrant, A., Lapierre, C., Pollet, B., Perre, P., 2009. Concomitant changes in viscoelastic properties and amorphous polymers during the hydrothermal treatment of hardwood and softwood. Journal of agricultural and food chemistry 57, 6830–6837.

Beall, F., 1971. Differential calometric analysis of wood and wood components. Wood science and technology 5, 159–175.

Boerjan, W., Ralph, J., Baucher, M., 2003. Lignin biosynthesis. Annual review of plant biology 54, 519–546.

Brachi, P., Miccio, F., Miccio, M., Ruoppolo, G., 2015. Isoconversional kinetic analysis of olive pomace decomposition under torrefaction operating conditions. Fuel Processing Technology 130, 147–154.

Cai, J., Liu, R., 2008. New distributed activation energy model: numerical solution and application to pyrolysis kinetics of some types of biomass. Bioresource technology 99, 2795–2799.

Cai, J., Wu, W., Liu, R., 2013a. Sensitivity analysis of three-parallel-daem-reaction model for describing rice straw pyrolysis. Bioresource Technology 132, 423–426.

Cai, J., Wu, W., Liu, R., 2014. An overview of distributed activation energy model and its application in the pyrolysis of lignocellulosic biomass. Renewable and Sustainable Energy Reviews 36, 236–246.

Cai, J., Wu, W., Liu, R., Huber, G.W., 2013b. A distributed activation energy model for the pyrolysis of lignocellulosic biomass. Green Chemistry 15, 1331–1340.

de Caprariis, B., Santarelli, M.L., Scarsella, M., Herce, C., Verdone, N., De Filippis, P., 2015. Kinetic analysis of biomass pyrolysis using a double distributed activation energy model. Journal of Thermal Analysis and Calorimetry 121, 1403–1410.

Cavagnol, S., Roesler, J.F., Sanz, E., Nastoll, W., Lu, P., Perré, P., 2015. Exothermicity in wood torrefaction and its impact on product mass yields: From micro to pilot scale. Canadian Journal of Chemical Engineering 93, 331–339.

Cavagnol, S., Sanz, E., Nastoll, W., Roesler, J.F., Zymla, V., Perré, P., 2013. Inverse analysis of wood pyrolysis with long residence times in the temperature range 210–290 c: Selection of multi-step kinetic models based on mass loss residues. Thermochimica acta 574, 1–9.

Chen, T., Zhang, J., Wu, J., 2016. Kinetic and energy production analysis of pyrolysis of lignocellulosic biomass using a three-parallel gaussian reaction model. Bioresource technology 211, 502–508.

Chen, W.H., Kuo, P.C., 2010. A study on torrefaction of various biomass materials and its impact on lignocellulosic structure simulated by a thermogravimetry. Energy 35, 2580–2586.

Chen, W.H., Kuo, P.C., 2011. Torrefaction and co-torrefaction characterization of hemicellulose, cellulose and lignin as well as torrefaction of some basic constituents in biomass. Energy 36, 803–811.

Chen, Z., Hu, M., Zhu, X., Guo, D., Liu, S., Hu, Z., Xiao, B., Wang, J., Laghari, M., 2015. Characteristics and kinetic study on pyrolysis of five lignocellulosic biomass via thermogravimetric analysis. Bioresource technology 192, 441–450.

Chornet, E., Roy, C., 1980. Compensation effect in the thermal decomposition of cellulosic materials. Thermochimica Acta 35, 389–393.

Cordero, T., Rodriguez-Maroto, J., Rodriguez-Mirasol, J., Rodriguez, J., 1990. On the kinetics of thermal decomposition of wood and wood components. Thermochimica Acta 164, 135–144.

Czajka, K., Kisiela, A., Moroń, W., Ferens, W., Rybak, W., 2016. Pyrolysis of solid fuels: Thermochemical behaviour, kinetics and compensation effect. Fuel Processing Technology 142, 42–53.

Demirbas, A., 2008. Biofuels sources, biofuel policy, biofuel economy and global biofuel projections. Energy conversion and management 49, 2106–2116.

Di Blasi, C., 2008. Modeling chemical and physical processes of wood and biomass pyrolysis. Progress in energy and combustion science 34, 47–90.

Di Blasi, C., Branca, C., Masotta, F., De Biase, E., 2013. Experimental analysis of reaction heat effects during beech wood pyrolysis. Energy & fuels 27, 2665–2674.

Di Blasi, C., Lanzetta, M., 1997. Intrinsic kinetics of isothermal xylan degradation in inert atmosphere. Journal of Analytical and Applied Pyrolysis 40, 287–303.

Ditmars, D., Ishihara, S., Chang, S., Bernstein, G., West, E., 1982. Enthalpy and heat-capacity standard reference material: synthetic sapphire (a-al2o3) from 10 to 2250 k. J Res Natl Bur Stand 87, 159–63.

Febrero, L., Granada, E., Pérez, C., Patiño, D., Arce, E., 2014. Characterisation and comparison of biomass ashes with different thermal histories using tg-dsc. Journal of Thermal Analysis and Calorimetry 118, 669–680.

Fisher, T., Hajaligol, M., Waymack, B., Kellogg, D., 2002. Pyrolysis behavior and kinetics of biomass derived materials. Journal of analytical and applied pyrolysis 62, 331–349.

Frederick Jr, W., Mentzer, C., 1975. Determination of heats of volatilization for polymers by differential scanning calorimetry. Journal of Applied Polymer Science 19, 1799–1804.

Grønli, M., Antal, M.J., Varhegyi, G., 1999. A round-robin study of cellulose pyrolysis kinetics by thermogravimetry. Industrial and Engineering Chemistry Research 38, 2238–2244.

Guo, W., Lim, C.J., Bi, X., Sokhansanj, S., Melin, S., 2013. Determination of effective thermal conductivity and specific heat capacity of wood pellets. Fuel 103, 347–355.

Haykiri-Acma, H., Yaman, S., Kucukbayrak, S., 2010. Comparison of the thermal reactivities of isolated lignin and holocellulose during pyrolysis. Fuel Processing Technology 91, 759–764.

Kan, T., Strezov, V., Evans, T.J., 2016. Lignocellulosic biomass pyrolysis: A review

of product properties and effects of pyrolysis parameters. Renewable and Sustainable Energy Reviews 57, 1126–1140.

Kifani-Sahban, F., Kifani, A., Belkbir, L., Belkbir, A., Zoulalian, A., Arauzo, J., Cardero, T., 1997. A physical approach in the understanding of the phenomena accompanying the thermal treatment of lignin. Thermochimica Acta 298, 199–204.

Kung, H.C., Kalelkar, A.S., 1973. On the heat of reaction in wood pyrolysis. Combustion and flame 20, 91–103.

Li, M., Liu, L., Jiang, L., Gou, F.H., Sun, J.H., 2019. Application of distributed activation energy models to polymer pyrolysis: Effects of distributed model selection, characteristics, validation, and sensitivity analysis. Fuel 254, 115594.

Lin, Y., Chen, Z., Dai, M., Fang, S., Liao, Y., Yu, Z., Ma, X., 2018. Co-pyrolysis kinetics of sewage sludge and bagasse using multiple normal distributed activation energy model (m-daem). Bioresource technology 259, 173–180.

Lin, Y., Tian, Y., Xia, Y., Fang, S., Liao, Y., Yu, Z., Ma, X., 2019. General distributed activation energy model (g-daem) on co-pyrolysis kinetics of bagasse and sewage sludge. Bioresource technology 273, 545–555.

Lv, P., Almeida, G., Perré, P., 2012. Torrefaction of cellulose: validity and limitation of the temperature/duration equivalence. Bioresources 7, 3720–3731.

Lv, P., Almeida, G., Perré, P., 2015. TGA-FTIR analysis of torrefaction of lignocellulosic components (cellulose, xylan, lignin) in isothermal conditions over a wide range of time durations. BioResources 10, 4239–4251.

McKendry, P., 2002. Energy production from biomass (part 1): overview of biomass. Bioresource Technology 83, 37–46.

Mishra, R.K., Mohanty, K., 2018. Pyrolysis kinetics and thermal behavior of waste sawdust biomass using thermogravimetric analysis. Bioresource technology 251, 63–74.

Miura, K., 1995. A new and simple method to estimate f (e) and k0 (e) in the distributed activation energy model from three sets of experimental data. Energy & Fuels 9, 302–307.

Navarro, M.V., Murillo, R., Mastral, A.M., Puy, N., Bartroli, J., 2009. Application of the distributed activation energy model to biomass and biomass constituents devolatilization. AIChE Journal 55, 2700–2715.

Nelder, J.A., Mead, R., 1965. A simplex method for function minimization. The Computer Journal 7, 308–313.

Perre, P., 2019. Coupled heat and mass transfer in biosourced porous media without local equilibrium: A macroscopic formulation tailored to computational simulation. International Journal of Heat and Mass Transfer 140, 717–730.

Perré, P., Rémond, R., Turner, I., 2013. A comprehensive dual-scale wood torrefaction model: Application to the analysis of thermal run-away in industrial heat treatment processes. International Journal of Heat and Mass Transfer 64, 838–849.

Poletto, M., Zattera, A.J., Forte, M.M., Santana, R.M., 2012. Thermal decomposition of wood: Influence of wood components and cellulose crystallite size. Bioresource Technology 109, 148–153.

Prins, M.J., Ptasinski, K.J., Janssen, F.J., 2006. Torrefaction of wood: Part 1. weight loss kinetics. Journal of analytical and applied pyrolysis 77, 28–34.

Ramiah, M., 1970. Thermogravimetric and differential thermal analysis of cellulose, hemicellulose, and lignin. Journal of Applied Polymer Science 14, 1323–1337.

Rath, J., Wolfinger, M.G., Steiner, G., Krammer, G., Barontini, F., Cozzani, V., 2003. Heat of wood pyrolysis. Fuel 82, 81–91.

Reed, T.B., Gaur, S., 1997. The High Heat of Fast Pyrolysis for Large Particles.

Rousset, P., Lapierre, C., Pollet, B., Quirino, W., Perre, P., 2009. Effect of severe thermal treatment on spruce and beech wood lignins. Annals of Forest Science 66, 1.

Rousset, P., Turner, I., Donnot, A., Perré, P., 2006. Choix d'un modèle de pyrolyse ménagée du bois à l'échelle de la microparticule en vue de la modélisation macroscopique. Annals of Forest Science 63, 213–229.

Sfakiotakis, S., Vamvuka, D., 2015. Development of a modified independent parallel reactions kinetic model and comparison with the distributed activation energy model for the pyrolysis of a wide variety of biomass fuels. Bioresource technology 197, 434–442.

Shafizadeh, F., 1985. Pyrolytic reactions and products of biomass, in: Fundamentals of thermochemical biomass conversion. Springer, pp. 183–217.

Shen, D., Gu, S., Jin, B., Fang, M., 2011. Thermal degradation mechanisms of wood under inert and oxidative environments using daem methods. Bioresource technology 102, 2047–2052.

Sonobe, T., Worasuwannarak, N., 2008. Kinetic analyses of biomass pyrolysis using the distributed activation energy model. Fuel 87, 414–421.

Soria-Verdugo, A., Goos, E., García-Hernando, N., 2015. Effect of the number of tga curves employed on the biomass pyrolysis kinetics results obtained using the distributed activation energy model. Fuel Processing Technology 134, 360–371.

Suwardie, J., Artiaga, R., 2000. The determination of heat of curing accompanied by reactant volatilization using simultaneous thermal analysis (STA). Thermochimica acta 357, 205–210.

Teng, H., Wei, Y.C., 1998. Thermogravimetric studies on the kinetics of rice hull pyrolysis and the influence of water treatment. Industrial and Engineering Chemistry Research 37, 3806–3811.

Thurner, F., Mann, U., 1981. Kinetic investigation of wood pyrolysis. Industrial and Engineering Chemistry Process Design and Development 20, 482–488.

Tinney, E.R., 1965. The combustion of wooden dowels in heated air, in: Symposium (International) on Combustion, Elsevier. pp. 925–930.

Turner, I., Rousset, P., Rémond, R., Perré, P., 2010. An experimental and theoretical investigation of the thermal treatment of wood *(Fagus sylvatica L.)* in the range 200–260°C. International Journal of Heat and Mass Transfer 53, 715–725.

Vand, V., 1943. A theory of the irreversible electrical resistance changes of metallic films evaporated in vacuum. Proceedings of the Physical Society 55, 222.

Varhegyi, G., Antal Jr, M.J., Szekely, T., Szabo, P., 1989. Kinetics of the thermal decomposition of cellulose, hemicellulose, and sugarcane bagasse. Energy & fuels 3, 329–335.

Varhegyi, G., Jakab, E., Antal Jr, M.J., 1994. Is the broido-shafizadeh model for cellulose pyrolysis true? Energy & fuels 8, 1345–1352.

Vassilev, S.V., Baxter, D., Andersen, L.K., Vassileva, C.G., 2013. An overview of the composition and application of biomass ash. part 1. phase–mineral and chemical composition and classification. Fuel 105, 40–76.

Wagenaar, B., Prins, W., van Swaaij, W.P.M., 1993. Flash pyrolysis kinetics of pine wood. Fuel Processing Technology 36, 291–298.

Wang, J., Lian, W., Li, P., Zhang, Z., Yang, J., Hao, X., Huang, W., Guan, G., 2017a. Simulation of pyrolysis in low rank coal particle by using daem kinetics model: Reaction behavior and heat transfer. Fuel 207, 126–135.

Wang, S., Dai, G., Yang, H., Luo, Z., 2017b. Lignocellulosic biomass pyrolysis mechanism: a state-of-the-art review. Progress in Energy and Combustion Science 62, 33–86.

Ward, S., Braslaw, J., 1985. Experimental weight loss kinetics of wood pyrolysis under vacuum. Combustion and Flame 61, 261–269.

Whetten, R.W., MacKay, J.J., Sederoff, R.R., 1998. Recent advances in understanding lignin biosynthesis. Annual Review of Plant Biology 49, 585–609.

White, J.E., Catallo, W.J., Legendre, B.L., 2011. Biomass pyrolysis kinetics: a comparative critical review with relevant agricultural residue case studies. Journal of Analytical and Applied Pyrolysis 91, 1–33.

Xu, D., Chai, M., Dong, Z., Rahman, M.M., Yu, X., Cai, J., 2018. Kinetic compensation effect in logistic distributed activation energy model for lignocellulosic biomass pyrolysis. Bioresource Technology 265, 139–145.

Xu, F., Yu, J., Tesso, T., Dowell, F., Wang, D., 2013. Qualitative and quantitative analysis of lignocellulosic biomass using infrared techniques: a mini-review. Applied Energy 104, 801–809.

Yang, H., Yan, R., Chen, H., Lee, D.H., Zheng, C., 2007. Characteristics of hemicellulose, cellulose and lignin pyrolysis. Fuel 86, 1781–1788.